H1prelim-08-013 Submitted to

XVI International Workshop on Deep-Inelastic Scattering, DIS2008, April 7-11, 2008, London
Parallel Session **Diffraction**

Electronic Access:https://www-h1.desy.de/publications/H1preliminary.short_list.html

Diffractive electroproduction of ρ and ϕ mesons at HERA-1

H1 Collaboration

Abstract

This paper reports on the H1 analysis of HERA-1 data for ρ and ϕ VM diffractive production, both in the elastic and proton dissociative channel. The analysed data, which correspond to 51 pb^{-1}, include a total of 12500 events in the transition region from low Q^2 to the perturbative domain, $2.5 < Q^2 < 60\ \mathrm{GeV}^2$, with data analysed in a consistent way, in particular for background estimates. The total, longitudinal and transverse cross sections are measured as a function of Q^2, W and $|t|$. The polarisation efects are discussed in detail, in particular the Q^2, $|t|$ and (for ρ mesons) $m_{\pi\pi}$ dependences of the s-channel helicity conserving and violating amplitudes and phases. A consistent picture of VM production at intermediate and large Q^2 thus emerges from H1 HERA-1 measurements, which can be interpreted in a QCD framework.

1 Introduction

This analysis is devoted to the study of diffractive electroproduction of ρ and ϕ vector mesons (designed in the following as VM), in the elastic and in the proton dissociative channels:

$$\begin{aligned} e + p &\rightarrow e + Y + VM \\ \rho &\rightarrow \pi^+ + \pi^- \ \ (\mathrm{BR} \simeq 100\%) \\ \phi &\rightarrow K^+ + K^- \ \ (\mathrm{BR} = 49.2 \pm 0.6\%), \end{aligned} \tag{1}$$

where Y represents the elastically scattered proton or a diffractively excited baryonic system, well separated in rapidity from the vector meson.

The data analysed here were taken by H1 from 1996 to 2000, which corresponds to $\approx 90\%$ of the data collected by H1 before the luminosity upgrade in 2002 ("HERA-1" data set). The interacting particles were electrons or positrons [1] of energy 27.5 GeV, colliding with 820 or 920 GeV protons, which corresponds to electron-proton centre of mass energies of $\sqrt{s} = 300$ and 320 GeV, respectively. The effective luminosity used for this analysis is of 51 pb^{-1}.

The kinematic domain of the measurement is:

$$\begin{aligned} 2.5 < Q^2 &< 60 \ \mathrm{GeV}^2 \\ 35 < W &< 180 \ \mathrm{GeV} \\ |t| &< 3 \ \mathrm{GeV}^2 \\ M_Y &< 5 \ \mathrm{GeV/c}^2, \end{aligned} \tag{2}$$

where $Q^2 = -q^2$, q being the virtual photon four-momentum, $W \simeq Q^2/x$ is the photon-proton centre of mass energy (x is the Bjorken scaling variable) and t is the square of the four-momentum transfer from the incident proton to the scattered system Y, of which the mass is M_Y.

2 Cross section measurements

The measurements of diffractive ρ and ϕ meson electroproduction cross sections, at Born level, are presented and discussed in this section for the elastic and for the proton dissociation processes.

They are presented in terms of $\gamma^\star p$ cross sections, as extracted from the ep cross sections in the Weiszacker-Williams equivalent photon approximation using the relation

$$\frac{\mathrm{d}^2\sigma(ep \rightarrow eVY)}{\mathrm{d}y \ \mathrm{d}Q^2} = \Gamma \ \sigma(\gamma^* p \rightarrow VY), \tag{3}$$

where the flux Γ of virtual photons and the inelasticity y are given by

$$\Gamma = \frac{\alpha_{em}}{\pi} \frac{1 - y + y^2/2}{y \ Q^2}, \qquad y = \frac{p \cdot q}{p \cdot k}, \tag{4}$$

α_{em} being the fine structure constant and p and k the 4-momenta of the incident proton and of the incident electron, respectively.

[1] In the rest of this paper, the word "electron" will be generically used for electron and positron.

2.1 Q^2 dependences

2.1.1 Total cross sections

The measurements of elastic and proton dissociative $\gamma^* p$ cross sections of ρ and ϕ mesons, in the elastic and the proton dissociation channels, are presented in Fig. 1 as a function of the scaling variable $(Q^2 + M_V^2)$, for $W = 75$ GeV.

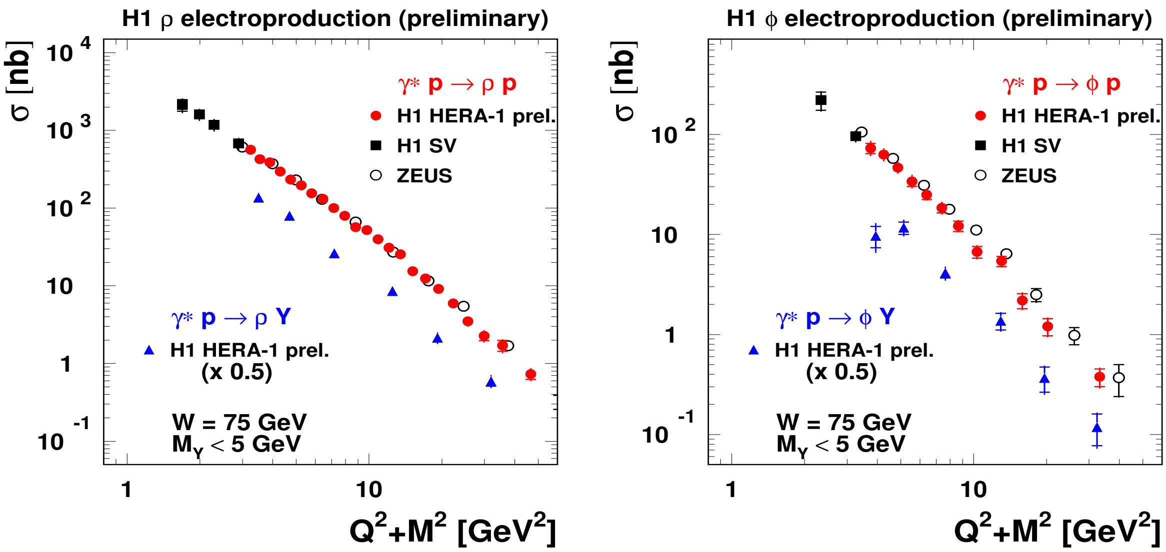

Figure 1: $(Q^2 + M_V^2)$ dependence of the $\gamma^* p \to VY$ cross sections for $W = 75$ GeV: (a) ρ meson production; (b) ϕ production. The upper points are for the elastic processes, the lower points for proton dissociative diffraction, divided by a factor 2 to improve the readability of the figures. Overall normalisation errors of 4.7% for ρ and 5.4% for ϕ mesons are not included in the error bars. H1 measurements of ρ [1] and ϕ [2] electroproduction at low Q^2 (shifted vertex, SV) and ZEUS measurements of ρ [8] and ϕ [10] electroproduction are also shown (the ZEUS ρ measurement was ported to $W = 75$ GeV using the W dependence measured by ZEUS).

2.1.2 Proton dissociative to elastic cross section ratios; factorisation

Figure 2 presents, as a function of Q^2, the ratios of the elastic and proton dissociative $\gamma^* p$ cross sections for ρ and ϕ mesons, for the dissociative mass domain $M_Y < 5~\mathrm{GeV/c^2}$ defined in the present experiment.

2.1.3 ϕ to ρ total cross section ratio

Figure 3 displays the ϕ to ρ elastic cross section ratio, plotted as a function of Q^2 and of $(Q^2 + M_V^2)$. In these ratios, several uncertainties cancel, in particular those related to proton dissociation background subtraction.

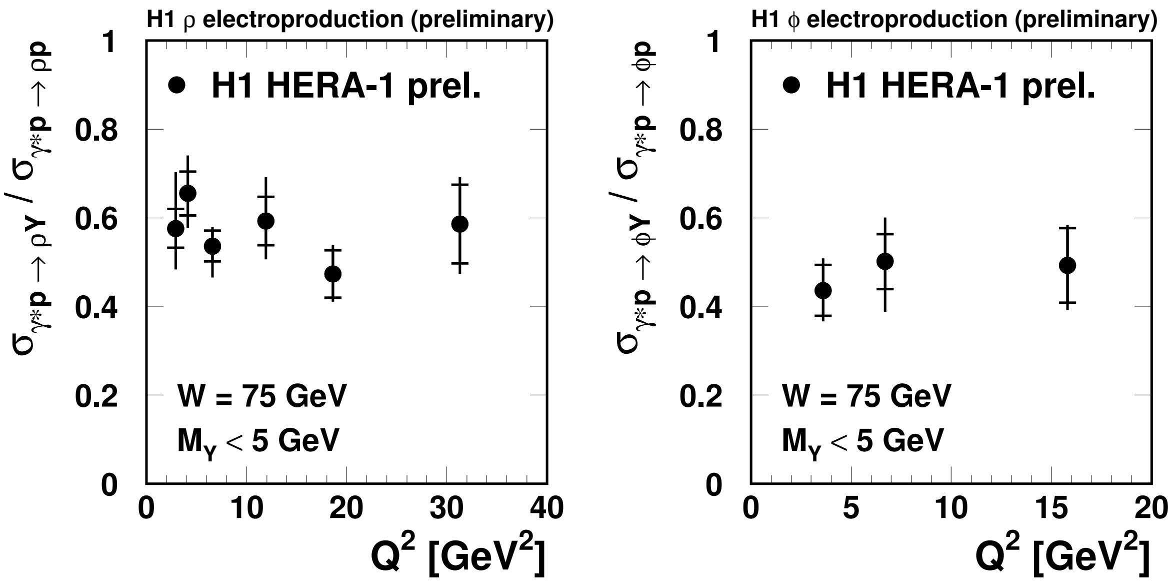

Figure 2: Q^2 dependence of the ratio of proton dissociative to elastic $\gamma^* p$ cross sections for $W = 75$ GeV: (a) ρ; (b) ϕ production. The overall normalisation error on the ratios, which is not included in the error bars, is 4%.

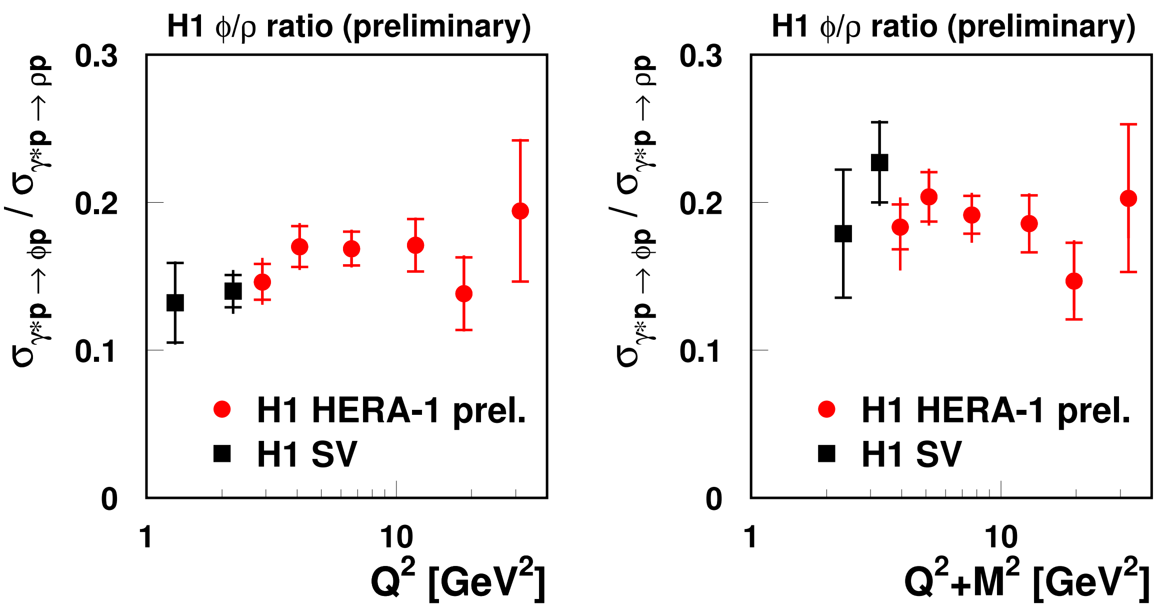

Figure 3: Ratio of the ϕ to ρ cross sections for $W = 75$ GeV: (a) as a function of Q^2; (b) as a function of $(Q^2 + M_V^2)$. The overall normalisation errors on the ratios, which are not included in the error bars, are of 4%. H1 measurements of ρ [1] and ϕ [2] electroproduction at low Q^2 (shifted vertex, SV) are also shown

2.1.4 Polarised cross sections

The $\gamma^* p$ cross section can be expressed as the sum of the contributions of transversely and longitudinally polarised virtual photons:

$$\sigma(\gamma^* p \to VY) = (\sigma_T + \varepsilon \sigma_L)\,(\gamma^* p \to VY) = \sigma_T(\gamma^* p \to VY)\,(1 + \varepsilon R), \tag{5}$$

where ε is the photon polarisation parameter given by $\varepsilon \simeq (1-y) / (1-y+y^2/2)$, with $0.91 < \varepsilon < 1.00$, $\langle \varepsilon \rangle = 0.98$ in the present data.

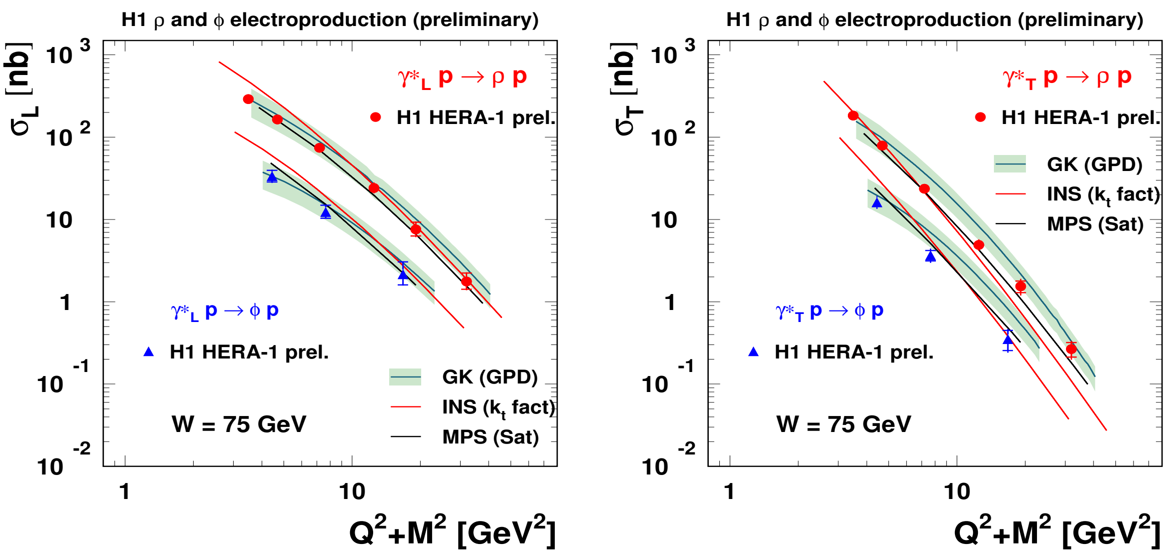

Figure 4: $(Q^2+M_V^2)$ dependences of (a) longitudinal and (b) transverse $\gamma^* p$ cross sections for elastic ρ and ϕ meson production with $W = 75$ GeV. The error bars include the error on the cross section ratio R. Overall normalisation errors of 4.7% for ρ and 5.4% for ϕ mesons are not included in the error bars. The superimposed curves are predictions from the models of ref. [13] (Grey area), of ref. [12] (red line) and of ref. [14] (black line).

The longitudinal and transverse cross sections are presented in Fig. 4 for elastic ρ and ϕ production, using the total cross section measurements, the cross section ratio $R = \sigma_L / \sigma_T$ obtained in section 3.2 from measurements of the spin density matrix elements, and the value of ε in the bin; the error on R is propagated to the polarised cross sections.

2.2 *W* dependences

Figure 5 displays the W dependences of elastic $\gamma^* p$ cross sections for ρ and ϕ mesons, for several Q^2 values.

The W dependence of the cross sections is characterised by power law fits of the form

$$\sigma(\gamma^* p) \propto W^{\delta}, \tag{6}$$

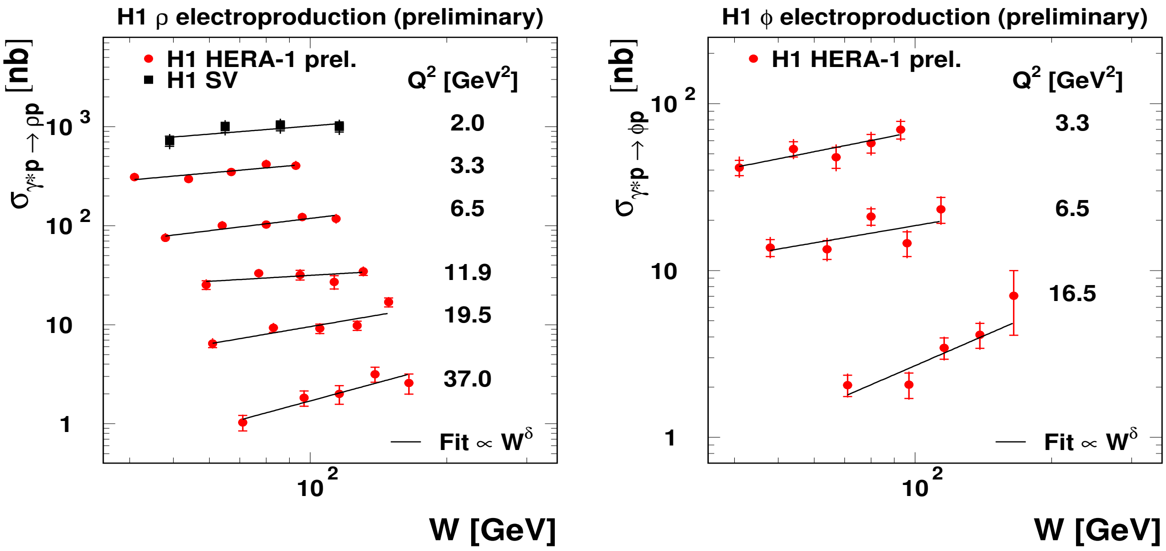

Figure 5: W dependences of the (a) ρ and (b) ϕ elastic $\gamma^* p \to VY$ cross sections, for several Q^2 values. Overall normalisation errors of 4.7% for ρ and 5.4% for ϕ mesons are not included in the error bars. H1 measurements of ρ [1] electroproduction at low Q^2 (shifted vertex, SV) are also shown. The lines are fits to eq. (6).

represented by the lines in Fig. 5. This parameterisation is inspired by the Regge description of soft interactions, with

$$\delta \simeq 4\,(\alpha_{I\!P}(\langle t \rangle) - 1), \quad \alpha_{I\!P}(t) = \alpha_{I\!P}(0) + \alpha'\, t. \tag{7}$$

In soft interactions, typical values for the intercept and the slope of the Regge trajectory are $\alpha_{I\!P}(0) \simeq 1.08$ [15] and $\alpha' \simeq 0.25$ GeV^{-2} [16].

The W dependences of VM elastic cross sections are summarised in Fig. 6 in the form of the $(Q^2 + M_V^2)$ dependence of $\alpha_{I\!P}(0)$, for ρ, ϕ and J/ψ mesons and Deeply virtual Compton Scattering (DVCS).

2.3 $|t|$ dependences

The t distributions for ρ and ϕ elastic and proton dissociative productions are presented in Fig. 7 for different ranges in Q^2. These distributions are well described by empirical exponential laws of type $\mathrm{d}\sigma(\gamma^* p)\ /\ \mathrm{d}t\ \propto e^{-b\,|t|}$, which are represented on the figure by the superimposed lines.

The slope parameters b, extracted from exponential fits in the range $|t| \ \leq 0.5$ GeV^2 for elastic scattering and $|t| \ \leq 3$ GeV^2 for proton dissociation are presented as a function of $(Q^2 + M_V^2)$ in Fig. 8, together with other ρ, ϕ and J/ψ photo- and electroproduction results from H1 and ZEUS.

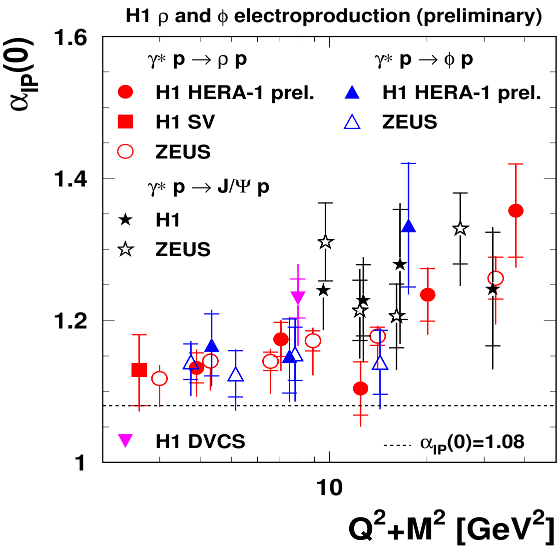

Figure 6: Evolution with $(Q^2 + M_V^2)$ of the parameter $\alpha_{I\!P}(0)$, extracted with the soft value $\alpha' = 0.25\ \mathrm{GeV}^{-2}$ and with $\alpha' = 0$ (no shrinkage – outer error bars), for ρ and ϕ elastic production. H1 low Q^2 ρ [1], J/ψ [4] and DVCS [5] measurements as well as ZEUS measurements for ρ [8], ϕ [10] and J/ψ [11] are also shown. Where relevant, original measurements of the parameter δ are transformed in measurements of $\alpha_{I\!P}(0)$ using $\alpha' = 0.25\ \mathrm{GeV}^{-2}$ and $\langle t \rangle = 1/b$. The value 1.08, typical for soft diffraction, is indicated by the dashed line.

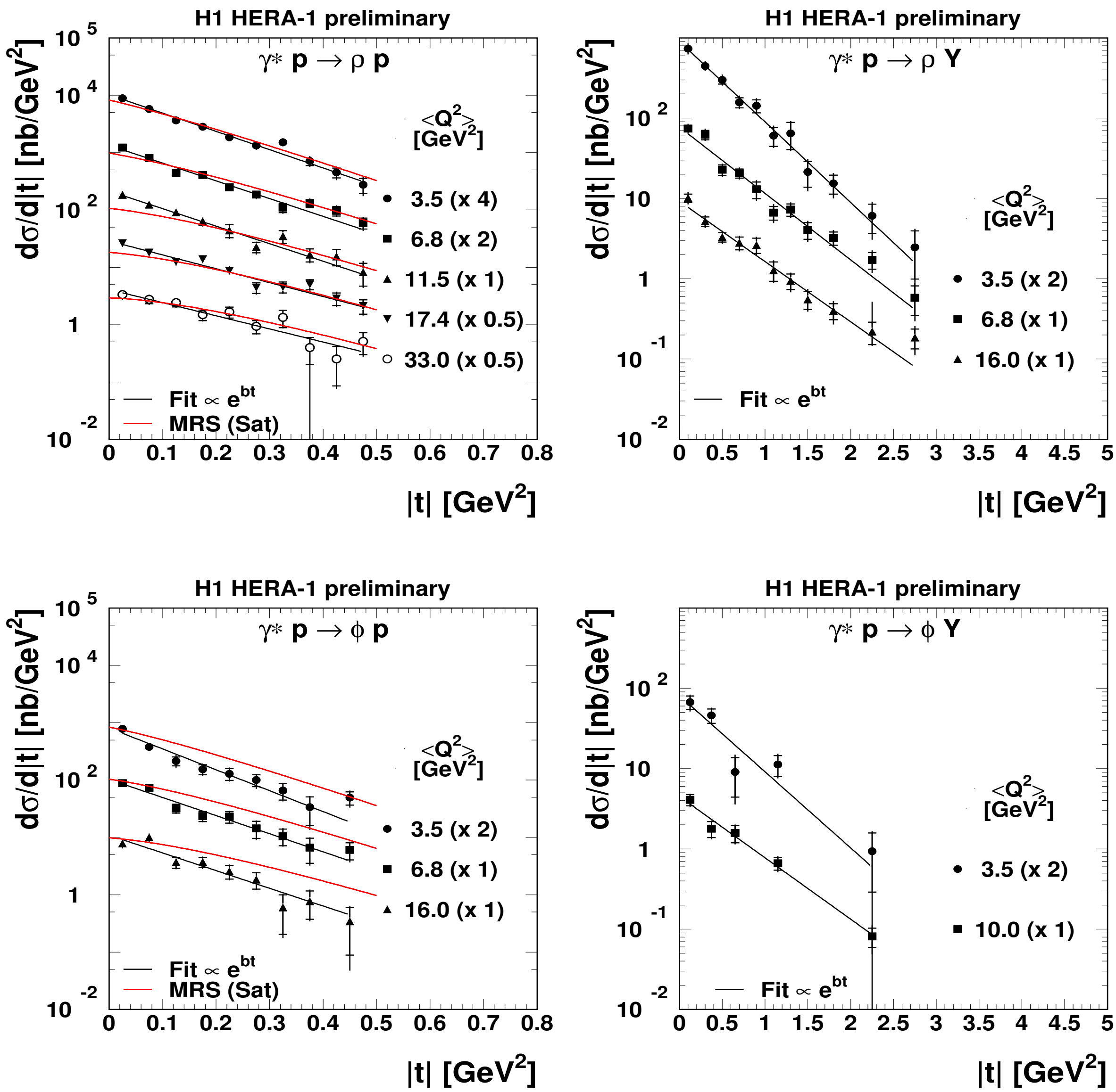

Figure 7: t dependences of the $\gamma^* p \to VY$ cross sections for several ranges in Q^2: (a) ρ and (b) ϕ elastic production; (c)-(d) proton dissociation. The distributions are multiplied by constant factors, to help readibility of the figures. The superimposed black lines correspond to exponential fits, over the indicated $|t|$ ranges. The superimposed red curves are predictions from the models of ref. [12].

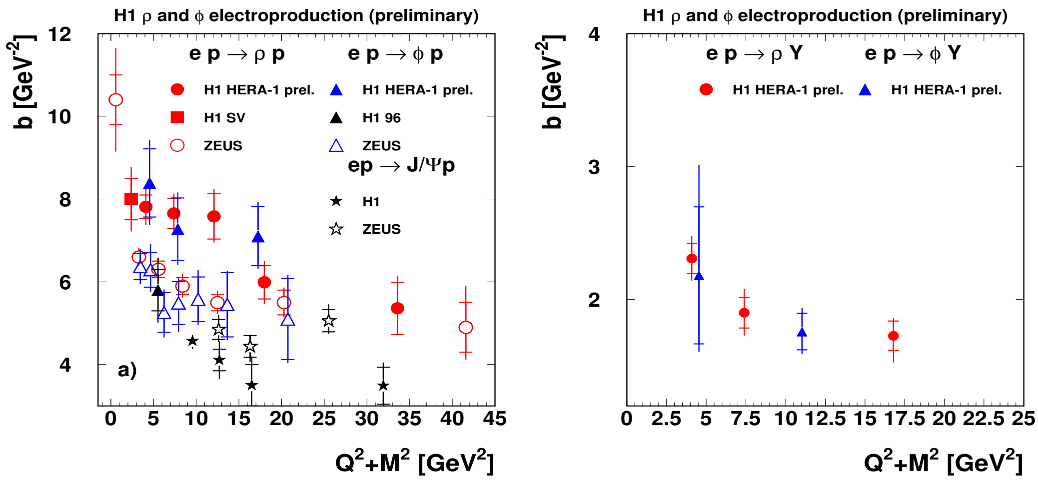

Figure 8: $(Q^2+M_V^2)$ dependences of the b slope parameters of the exponentially falling $|t|$ distributions of ρ and ϕ $\gamma^* p \to VY$ cross sections: (a) elastic scattering; (b) proton dissociation. H1 data for J/ψ production [4] and ZEUS data for ρ [6, 8], ϕ [9, 10] and J/ψ production [11] are also presented.

3 Polarisation measurements

The spin and parity properties of the exchange responsible for diffractive VM production are accessed through measurements of three angles characterising the VM decay into two pseudoscalar particles. In the helicity frame used for the present measurement, one is chosen as the azimuthal angle ϕ, which in the $\gamma^\star p$ centre of mass system is the angle between the electron scattering plane and the VM production plane (defined by the virtual photon and the VM directions). The other two angles, describing the vector meson decay, are chosen in the VM rest frame as the polar angle θ and the azimuthal angle φ of the positively charged decay particle, the quantization axis being directed oppositely to the outgoing Y system direction.

3.1 Spin density matrix elements

In the formalism presented in ref. [17], which is used extensively here, angular distributions allow the measurement of (complex) spin density matrix elements, which are bilinear combinations of the helicity amplitudes $T_{\lambda_V \lambda_{N'}, \lambda_\gamma \lambda_N}$, where λ_γ and λ_V are the helicities of the VM and of the virtual photon, respectively, and λ_N and $\lambda_{N'}$ the helicities of the incoming proton and of the outgoing baryonic system Y.

In the absence of longitudinal beam polarisation, 15 real or imaginary independent components of the spin density matrix are non-zero. They enter in the normalised angular distribution

$W(\theta, \varphi, \phi)$:

$$
\begin{aligned}
W(\theta, \varphi, \phi) = \frac{3}{4\pi} \; \Big\{ \; & \frac{1}{2}(1 - r^{04}_{00}) + \frac{1}{2}(3\, r^{04}_{00} - 1) \; \cos^2\theta \\
& -\sqrt{2}\, \mathrm{Re}\, r^{04}_{10} \; \sin 2\theta \cos\varphi - r^{04}_{1-1} \; \sin^2\theta \cos 2\varphi \\
& -\varepsilon \; \cos 2\phi \Big(r^{1}_{11} \; \sin^2\theta + r^{1}_{00} \; \cos^2\theta - \sqrt{2}\, \mathrm{Re}\, r^{1}_{10} \; \sin 2\theta \cos\varphi \\
& \qquad - r^{1}_{1-1} \; \sin^2\theta \cos 2\varphi \Big) \\
& -\varepsilon \; \sin 2\phi \Big(\sqrt{2}\, \mathrm{Im}\, r^{2}_{10} \; \sin 2\theta \sin\varphi + \mathrm{Im}\, r^{2}_{1-1} \; \sin^2\theta \sin 2\varphi \Big) \\
& +\sqrt{2\varepsilon\,(1+\varepsilon)} \; \cos\phi \; \Big(r^{5}_{11} \; \sin^2\theta + r^{5}_{00} \; \cos^2\theta \\
& \qquad -\sqrt{2}\, \mathrm{Re}\, r^{5}_{10} \; \sin 2\theta \cos\varphi - r^{5}_{1-1} \; \sin^2\theta \cos 2\varphi \Big) \\
& +\sqrt{2\varepsilon\,(1+\varepsilon)} \; \sin\phi \; \Big(\sqrt{2}\, \mathrm{Im}\, r^{6}_{10} \; \sin 2\theta \sin\varphi \\
& \qquad +\mathrm{Im}\, r^{6}_{1-1} \; \sin^2\theta \sin 2\varphi \Big) \Big\} .
\end{aligned}
\tag{8}
$$

The matrix elements can be measured as projections of the normalised angular distribution (8) onto specific orthogonal functions of the θ, φ and ϕ angles, one function corresponding to one matrix element (see ref. [17]).

Both for ρ and ϕ meson production, the matrix element measurements for the elastic and proton dissociative channels are found to be compatible within experimental errors. In order to improve the statistical significance of the measurements, elastic and proton dissociation event samples are combined in the following for $|t| < 0.5$ GeV^2; for $0.5 < |t| < 3$ GeV^2, the tag samples only are used, in view of the ρ' background among notag ρ events.

3.2 Cross section ratio $R = \sigma_L/\sigma_T$

Figure 13 presents the measurements of R as a function of Q^2 for ρ and ϕ mesons, and as a function of $m_{\pi\pi}$ for ρ mesons

3.3 Amplitude ratios

Assuming purely imaginary amplitudes, the relative strengths of the four amplitudes, with reference to the dominant T_{00} amplitude :

$$
\begin{aligned}
\alpha &= |T_{11}| \;/\; |T_{00}| \\
\beta &= |T_{01}| \;/\; |T_{00}| \\
\delta &= |T_{10}| \;/\; |T_{00}| \\
\eta &= |T_{-11}| \;/\; |T_{00}|
\end{aligned}
\tag{9}
$$

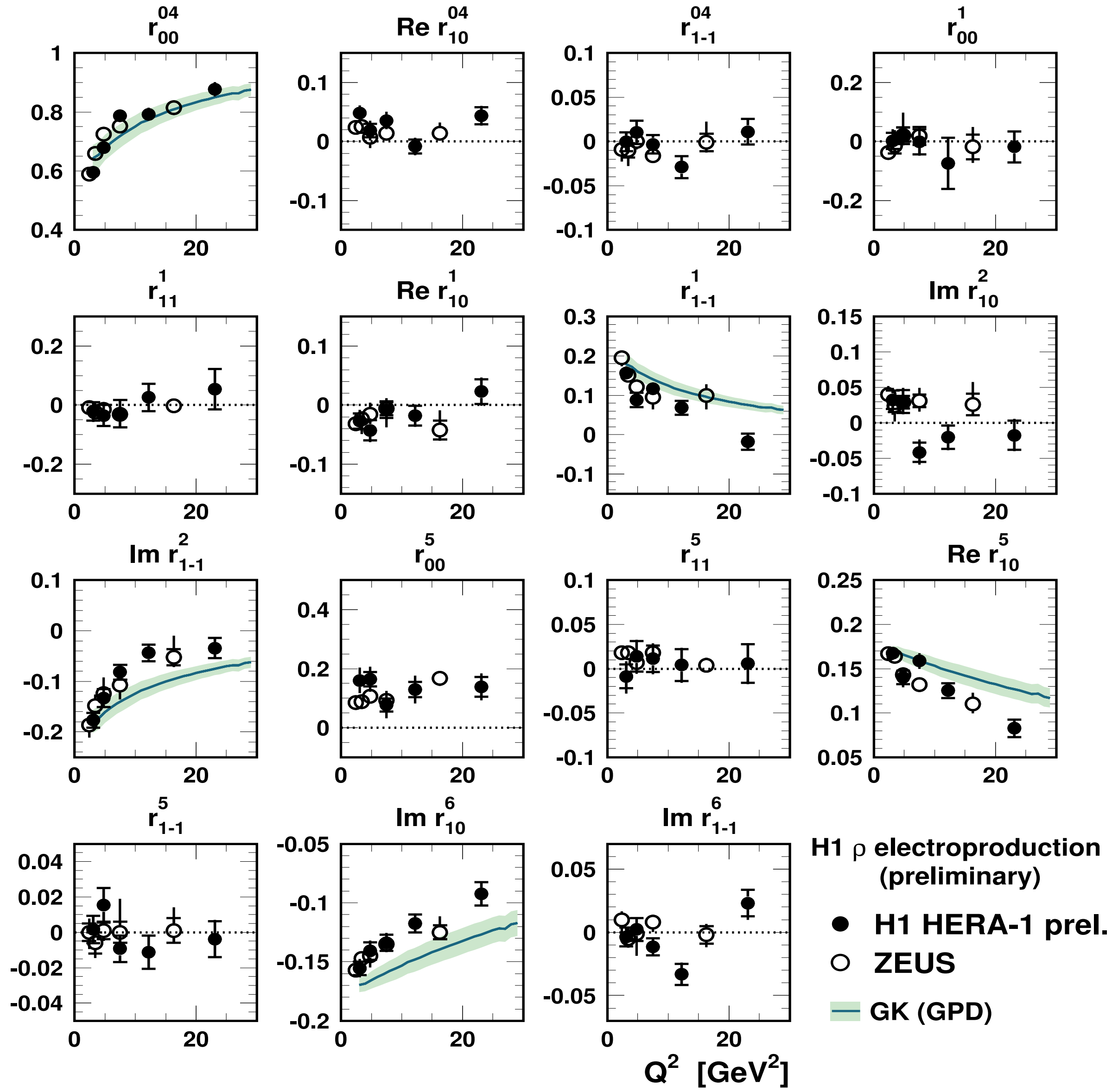

Figure 9: Spin density matrix elements for diffractive electroproduction of ρ mesons as a function of Q^2. The notag ($|t| < 0.5$ GeV^2) and tag ($|t| < 3$ GeV^2) samples are combined. The dashed lines show the expected vanishing expectation values for SCHC exchange. ZEUS results [8] are also shown. Model predictions [13] are superimposed to the data.

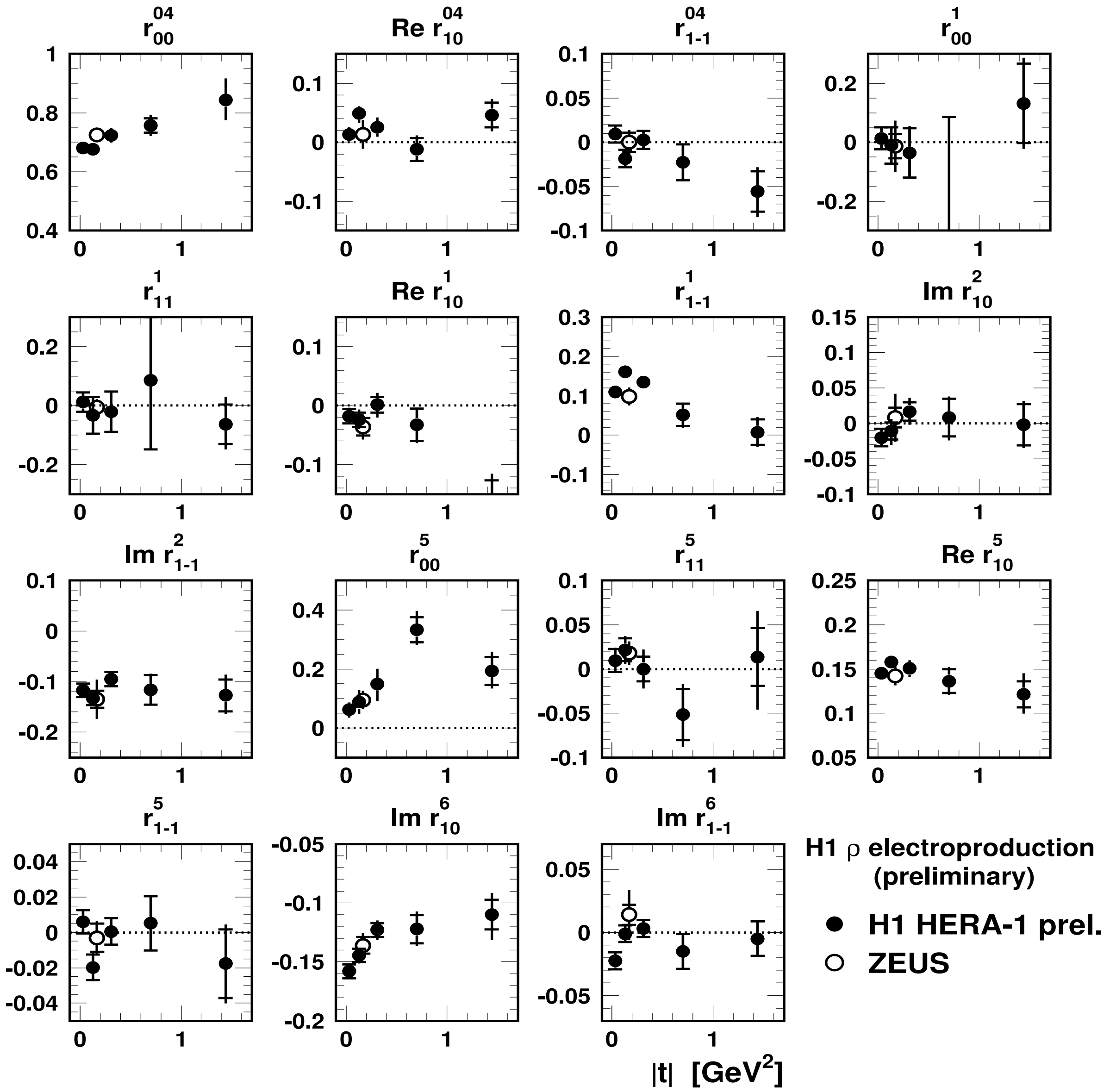

Figure 10: Spin density matrix elements for diffractive electroproduction of ϕ mesons as a function of $|t|$. The notag ($|t| < 0.5$ GeV^2) and tag ($|t| < 3$ GeV^2) samples are combined. The dashed lines show the expected vanishing expectation values for SCHC exchange. ZEUS results [7] are also shown.

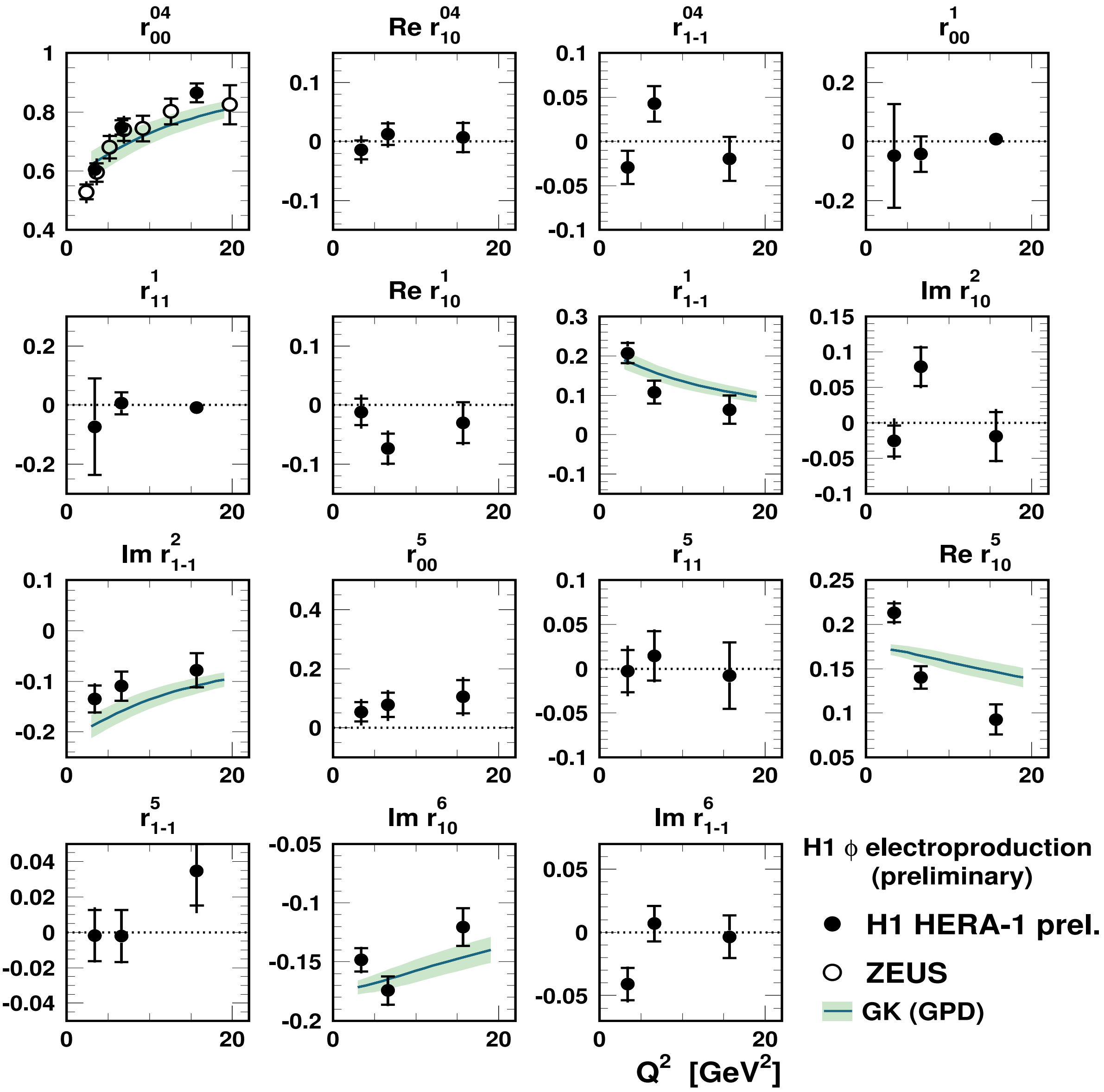

Figure 11: Spin density matrix elements for diffractive electroproduction of ϕ mesons as a function of Q^2. The notag ($|t| < 0.5$ GeV^2) and tag ($|t| < 3$ GeV^2) samples are combined. The dashed lines show the expected vanishing expectation values for SCHC exchange. ZEUS results [10] are also shown. Model predictions [13] are superimposed to the data.

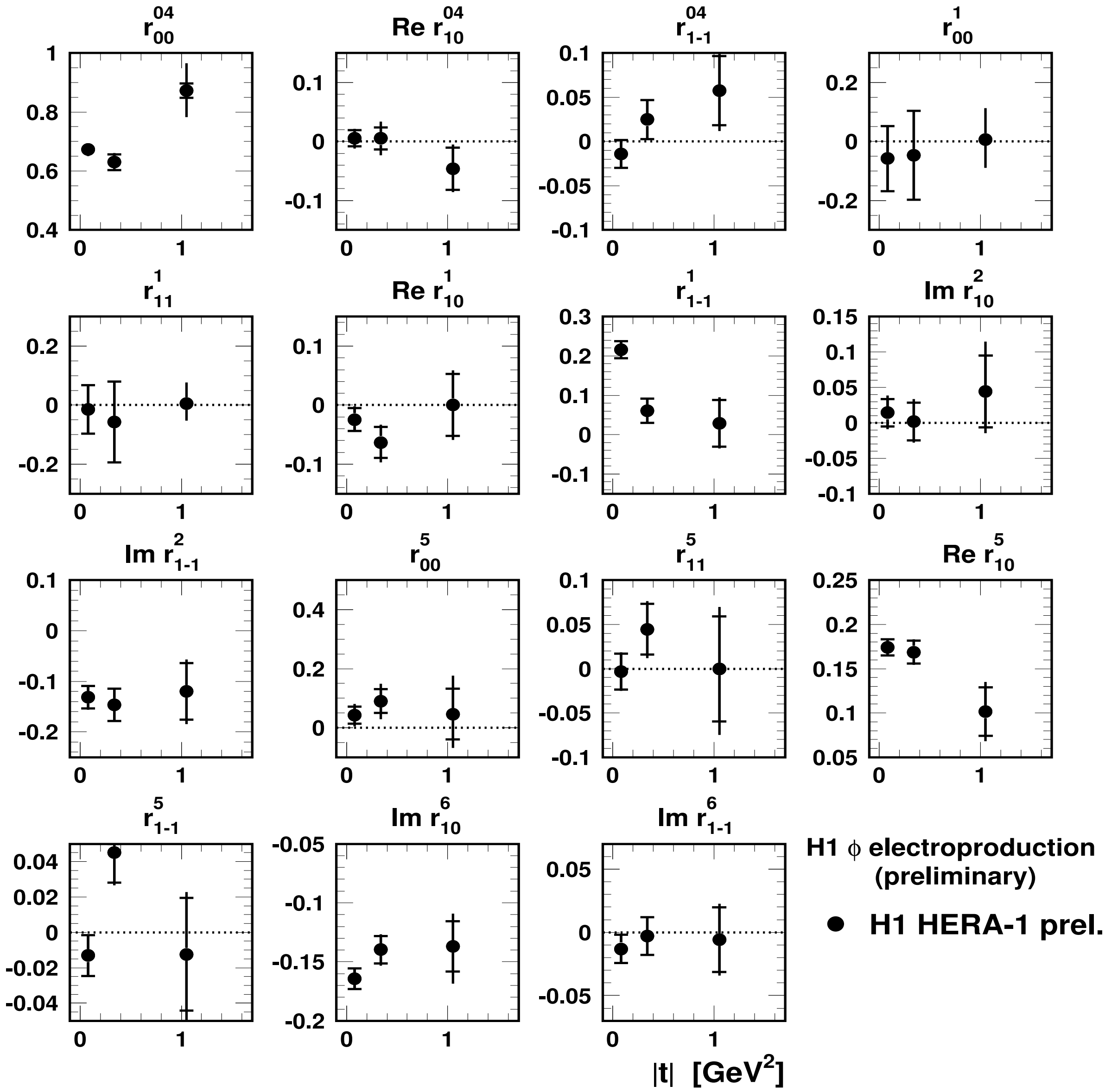

Figure 12: Spin density matrix elements for diffractive electroproduction of ϕ mesons as a function of $|t|$. The notag ($|t| < 0.5$ GeV^2) and tag ($|t| < 3$ GeV^2) samples are combined. The dashed lines show the expected vanishing expectation values for SCHC exchange.

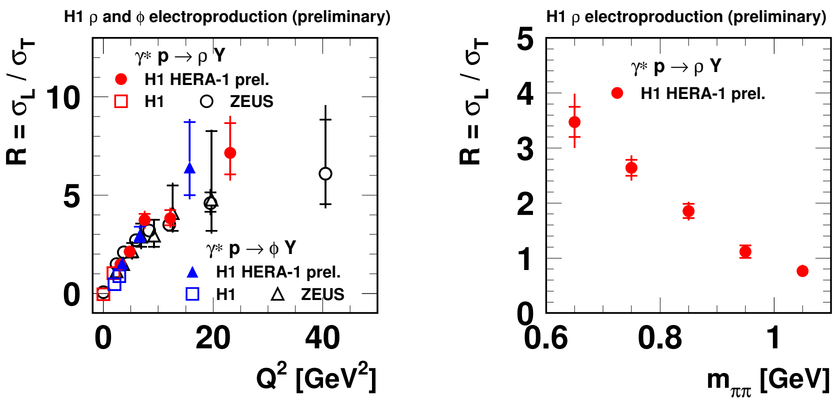

Figure 13: Ratio $R = \sigma_L$ / σ_T of the longitudinal and transverse cross sections, as a function of (a) Q^2 and (b) $|t|$ for ρ and ϕ meson diffractive production together with previous H1 [1–3] and ZEUS [6, 8, 10] measurements; (c) of $m_{\pi\pi}$ for ρ meson production. The notag ($|t| < 0.5\ \mathrm{GeV}^2$) and tag ($|t| < 3\ \mathrm{GeV}^2$) samples are combined.

can be computed from global fits to the measurements of the 15 matrix elements (see Appendix B) .

The fit results for the four amplitude ratios are presented in Figs. 14, as a function of Q^2 and $|t|$ for ρ and ϕ mesons. Negative values are allowed for α - η, the corresponding amplitudes being then supposed to be opposite in phase.

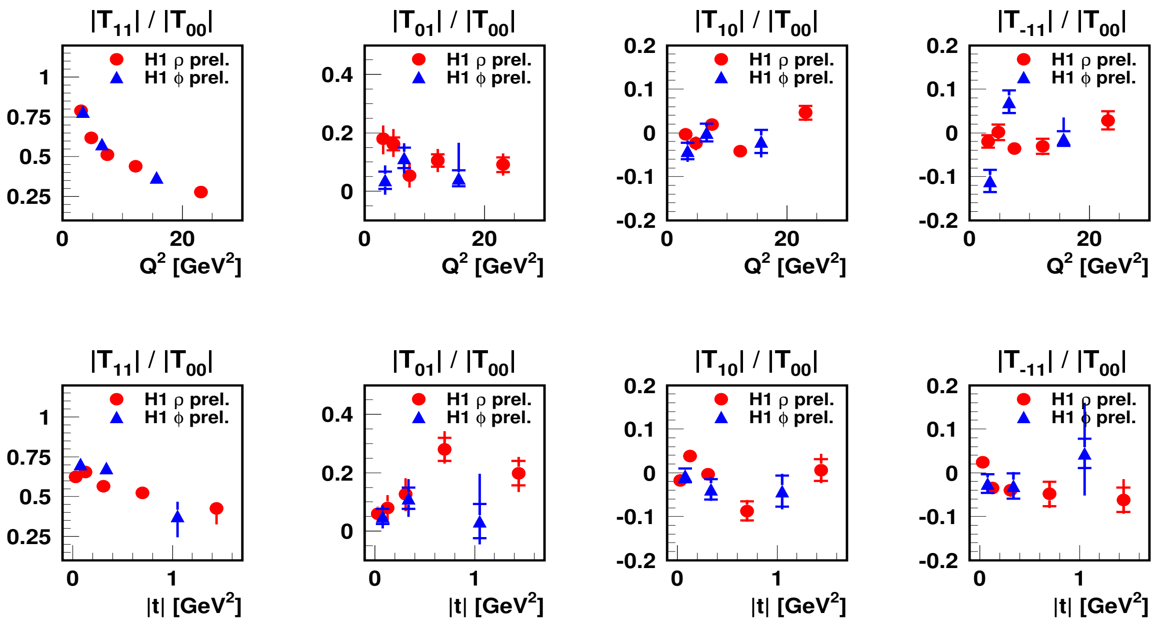

Figure 14: Amplitude ratios for ρ and ϕ production, computed from global fits to the measurements of the 15 matrix elements, as a function of Q^2 (upper row) and $|t|$ (lower row). The notag ($|t| < 0.5$ GeV^2) and tag ($|t| < 3$ GeV^2) samples are combined.

4 Appendix A

Spin density matrix elements relevant for VM electroproduction with unpolarised lepton beam, given in terms of helicity amplitudes $T_{\lambda_V\lambda_\gamma}$ (natural parity exchange is not assumed) [17]:

$$r^{04}_{00} = \frac{1}{1+\varepsilon R}\left[\frac{1}{2N_T}\left(|T_{01}|^2+|T_{0-1}|^2\right)+\frac{\varepsilon R}{N_L}|T_{00}|^2\right] \tag{10}$$

$$\mathrm{Re}\, r^{04}_{10} = \frac{1}{1+\varepsilon R}\,\mathrm{Re}\left[\frac{1}{2N_T}\left(T_{11}T^\dagger_{01}+T_{1-1}T^\dagger_{0-1}\right)+\frac{\varepsilon R}{N_L}T_{10}T^\dagger_{00}\right] \tag{11}$$

$$r^{04}_{1-1} = \frac{1}{1+\varepsilon R}\left[\frac{1}{2N_T}\left(T_{11}T^\dagger_{-11}+T_{1-1}T^\dagger_{-1-1}\right)+\frac{\varepsilon R}{N_L}T_{10}T^\dagger_{-10}\right] \tag{12}$$

$$r^{1}_{00} = \frac{1}{1+\varepsilon R}\,\frac{1}{2N_T}\left(T_{0-1}T^\dagger_{01}+T_{01}T^\dagger_{0-1}\right) \tag{13}$$

$$r^{1}_{11} = \frac{1}{1+\varepsilon R}\,\frac{1}{2N_T}\left(T_{1-1}T^\dagger_{11}+T_{11}T^\dagger_{1-1}\right) \tag{14}$$

$$\mathrm{Re}\, r^{1}_{10} = \frac{1}{1+\varepsilon R}\,\frac{1}{2N_T}\,\mathrm{Re}\left(T_{1-1}T^\dagger_{01}+T_{11}T^\dagger_{0-1}\right) \tag{15}$$

$$r^{1}_{1-1} = \frac{1}{1+\varepsilon R}\,\frac{1}{2N_T}\left(T_{1-1}T^\dagger_{-11}+T_{11}T^\dagger_{-1-1}\right) \tag{16}$$

$$\mathrm{Im}\, r^{2}_{10} = \frac{1}{1+\varepsilon R}\,\frac{1}{2N_T}\,\mathrm{Re}\left(T_{1-1}T^\dagger_{01}-T_{11}T^\dagger_{0-1}\right) \tag{17}$$

$$\mathrm{Im}\, r^{2}_{1-1} = \frac{1}{1+\varepsilon R}\,\frac{1}{2N_T}\,\mathrm{Re}\left(T_{1-1}T^\dagger_{-11}-T_{11}T^\dagger_{-1-1}\right) \tag{18}$$

$$r^{5}_{00} = \frac{\sqrt{R}}{1+\varepsilon R}\,\frac{1}{\sqrt{2N_TN_L}}\left[\mathrm{Re}\,(T_{00}T^\dagger_{01})-\mathrm{Re}\,(T_{00}T^\dagger_{0-1})\right] \tag{19}$$

$$r^{5}_{11} = \frac{\sqrt{R}}{1+\varepsilon R}\,\frac{1}{\sqrt{2N_TN_L}}\left[\mathrm{Re}\,(T_{10}T^\dagger_{11})-\mathrm{Re}\,(T_{10}T^\dagger_{1-1})\right] \tag{20}$$

$$\mathrm{Re}\, r^{5}_{10} = \frac{\sqrt{R}}{1+\varepsilon R}\,\frac{1}{\sqrt{2N_TN_L}}\,\frac{1}{2}\mathrm{Re}\left(T_{10}T^\dagger_{01}+T_{11}T^\dagger_{00}-T_{10}T^\dagger_{0-1}-T_{1-1}T^\dagger_{00}\right) \tag{21}$$

$$r^{5}_{1-1} = \frac{\sqrt{R}}{1+\varepsilon R}\,\frac{1}{\sqrt{2N_TN_L}}\,\frac{1}{2}\left(T_{10}T^\dagger_{-11}+T_{11}T^\dagger_{-10}-T_{10}T^\dagger_{-1-1}-T_{1-1}T^\dagger_{-10}\right) \tag{22}$$

$$\mathrm{Im}\, r^{6}_{10} = \frac{\sqrt{R}}{1+\varepsilon R}\,\frac{1}{\sqrt{2N_TN_L}}\,\frac{1}{2}\mathrm{Re}\left(T_{10}T^\dagger_{01}-T_{11}T^\dagger_{00}+T_{10}T^\dagger_{0-1}-T_{1-1}T^\dagger_{00}\right) \tag{23}$$

$$\mathrm{Im}\, r^{6}_{1-1} = \frac{\sqrt{R}}{1+\varepsilon R}\,\frac{1}{\sqrt{2N_TN_L}}\,\frac{1}{2}\mathrm{Re}\left(T_{10}T^\dagger_{-11}-T_{11}T^\dagger_{-10}+T_{10}T^\dagger_{-1-1}-T_{1-1}T^\dagger_{-10}\right) \tag{24}$$

where R is the longitudinal to transverse cross section ratio

$$R = \frac{N_L}{N_T}, \tag{25}$$

and

$$N_L = |T_{00}|^2+|T_{10}|^2+|T_{-10}|^2 \tag{26}$$

$$N_T = \frac{1}{2}\left[|T_{11}|^2+|T_{-1-1}|^2+|T_{01}|^2+|T_{0-1}|^2+|T_{-11}|^2+|T_{1-1}|^2\right]. \tag{27}$$

5 Appendix B

Spin density matrix elements relevant for VM electroproduction with unpolarised lepton beam, given in terms of amplitude ratios (natural parity exchange is assumed) [17, 18]:

$$
\begin{aligned}
r^{04}_{00} &= B\,(\varepsilon + \beta^2) && (28)\\
\mathrm{Re}\, r^{04}_{10} &= B/2\,(2\varepsilon\delta + \beta\alpha - \beta\eta) && (29)\\
r^{04}_{1-1} &= B\,(\alpha\eta - \varepsilon\delta^2) && (30)\\
r^{1}_{00} &= -B\,\beta^2 && (31)\\
r^{1}_{11} &= B\,\alpha\eta && (32)\\
\mathrm{Re}\, r^{1}_{10} &= B/2\,\beta(\eta - \alpha) && (33)\\
r^{1}_{1-1} &= B/2\,(\alpha^2 + \eta^2) && (34)\\
\mathrm{Im}\, r^{2}_{10} &= B/2\,\beta(\alpha + \eta) && (35)\\
\mathrm{Im}\, r^{2}_{1-1} &= B/2\,(\eta^2 - \alpha^2) && (36)\\
r^{5}_{00} &= \sqrt{2}B\,\beta && (37)\\
r^{5}_{11} &= B/\sqrt{2}\,\delta(\alpha - \eta) && (38)\\
\mathrm{Re}\, r^{5}_{10} &= B/(2\sqrt{2})\,(2\beta\delta + \alpha - \eta) && (39)\\
r^{5}_{1-1} &= B/\sqrt{2}\,\delta(\eta - \alpha) && (40)\\
\mathrm{Im}\, r^{6}_{10} &= -B/(2\sqrt{2})\,(\alpha + \eta) && (41)\\
\mathrm{Im}\, r^{6}_{1-1} &= B/\sqrt{2}\,\delta(\alpha + \eta) && (42)
\end{aligned}
$$

where

$$
\begin{aligned}
\alpha &= |T_{11}|\ /\ |T_{00}| && (43)\\
\beta &= |T_{01}|\ /\ |T_{00}| && (44)\\
\delta &= |T_{10}|\ /\ |T_{00}| && (45)\\
\eta &= |T_{-11}|\ /\ |T_{00}| && (46)
\end{aligned}
$$

and

$$
\begin{aligned}
B = \frac{1}{N_T + \varepsilon N_L} N_T &= \alpha^2 + \beta^2 + \eta^2 && (47)\\
N_L &= 1 + 2\delta^2. && (48)
\end{aligned}
$$

References

[1] C. Adloff *et al.* [H1 Collaboration], Eur. Phys. J. **C13** (2000) 371 [hep-ex/9902019].

[2] C. Adloff *et al.* [H1 Collaboration], Phys. Lett. **B483** (2000) 360 [hep-ex/0005010].

[3] S. Aid *et al.* [H1 Collaboration], Nucl. Phys. **B463** (1996) 3 [hep-ex/9601004].

[4] A. Aktas *et al.* [H1 Collaboration], Eur. Phys. J. **C46** (2006) 585 [hep-ex/0510016].

[5] A. Aktas et al., [H1 Collaboration], Eur. Phys. J. **C44** (2005) 1 [hep-ex/0505061].

[6] J. Breitweg *et al.* [ZEUS Collaboration], Eur. Phys. J. **C2** (1998) 247 [hep-ex/9712020]; M. Derrick *et al.* [ZEUS Collaboration], Z. Phys. **C69** (1995) 39 [hep-ex/9507011].

[7] J. Breitweg *et al.* [ZEUS Collaboration], Eur. Phys. J. **C 12** (2000) 393 [hep-ex/9908026].

[8] S. Chekanov *et al.* [ZEUS Collaboration], [hep-ex/0708.1478].

[9] M. Derrick *et al.* [ZEUS Collaboration], Phys. Lett. **B 377** (1996) 259 [hep-ex/9601009].

[10] S. Chekanov et al. [ZEUS Collaboration], Nucl. Phys. **B 718** (2005) 3 [hep-ex/0504010].

[11] S. Chekanov *et al.* [ZEUS Collaboration], Eur. Phys. J. **C24** (2002) 345 [hep-ex/0201043]; idem, Nucl. Phys. **B 695** (2004) 3 [hep-ex/0404008].

[12] I.P. Ivanov, N.N. Nikolaev and A.A. Savin, Phys.Part.Nucl. 37 (2006) 1.

[13] S.V. Goloskokov and P. Kroll, arXiv:hep-ph/0708.3569 (2007).

[14] C. Marquet, R. Peschanski and G. Soyez, Phys. Rev. **D76** (2007) 034011.

[15] A. Donnachie and P.V. Landshoff, *Phys. Lett.* **B296** (1992) 227; see also J.-R. Cudell, K. Kang and S. Kim, Phys. Lett. **B395** (1997) 311.

[16] Phys. Rev. **D10** (1974) 170;
Nucl. Phys. Proc. Suppl. **12** (1990) 397.

[17] K. Schilling and G. Wolf, Nucl. Phys. **B61** (1973) 381.

[18] D.Yu. Ivanov and R. Kirschner, Phys. Rev. **D58** (1998) 114026